Journal of Hazardous Materials 176 (2010) 495–502

Contents lists available at ScienceDirect

Journal of Hazardous Materials

journal homepage: www.elsevier.com/locate/jhazmat

On the photocatalytic properties of elongated TiO_2 nanoparticles for phenol degradation and Cr(VI) reduction

Rongxin Mu, Zhaoyi Xu, Liyuan Li, Yun Shao, Haiqing Wan, Shourong Zheng*

State Key Laboratory of Pollution Control and Resource Reuse, School of the Environment, Nanjing University, Nanjing 210093, PR China

ARTICLE INFO

Article history:
Received 8 October 2009
Received in revised form 7 November 2009
Accepted 9 November 2009
Available online 13 November 2009

Keywords:
TiO_2 nanofiber
Hydrothermal reaction
Post-treatment
Photocatalytic phenol degradation
Photocatalytic Cr(VI) reduction

ABSTRACT

Elongated TiO_2 nanoparticles with high aspect ratio have specific advantages in separation processes. In this study, TiO_2 nanofiber was prepared via a hydrothermal reaction, and TiO_2 nanoparticles with varied structural properties were obtained using hydrothermal and calcination post-treatments. Photocatalytic phenol degradation and Cr(VI) reduction over these catalysts was investigated. Results showed that hydrothermally prepared TiO_2 nanofiber consisted of titanate with high aspect ratio. Calcining the as-prepared TiO_2 nanofiber at 400 and 600 °C led to the crystalline phase transformation from titanate to TiO_2-B and to the presence of mixed crystalline phases composed of TiO_2-B and anatase. In contrast, hydrothermal post-treatment results in the generation of pure anatase TiO_2 nanoparticles. For photocatalytic phenol degradation, calcining the as-prepared TiO_2 nanofiber resulted in an enhanced catalytic activity, whereas TiO_2 nanoparticles obtained by calcination post-treatment showed lower catalytic activities for photocatalytic Cr(VI) reduction compared to as-prepared TiO_2 nanofiber. TiO_2 nanofiber modified using the hydrothermal post-treatment, however, exhibited the highest catalytic activity among TiO_2 nanoparticles examined for both photocatalytic phenol degradation and Cr(VI) reduction. Furthermore, TiO_2 nanoparticles obtained by hydrothermal post-treatment showed the best sedimentation efficiency, highlighting its prominent potential as a readily separable and recoverable photocatalyst.

1. Introduction

Since the discovery of photocatalytic water splitting and degradation of organic contaminants [1,2], photocatalytic abatement of environmental pollutants has attracted considerable interest from both academic and industrial societies. In principle, the photocatalytic reaction is implemented by the excitation of electrons from the valence band to the conduction band of the semiconductor upon light irradiation, by which the excited electrons and holes can be used in reduction and oxidation reactions, respectively. Therefore, photocatalysis process is believed to be capable of eliminating organic or inorganic pollutants in water via an oxidation or reduction mechanism [3–5].

TiO_2 has been considered as one of the most practical candidates due to its low toxicity, high stability and prominent catalytic efficiency [5]. From the viewpoint of field applications, however, the large band gap of TiO_2 and the difficulty in catalyst recovery are recognized to be the major disadvantages of powdered TiO_2 [3,6]. Preparation of supported photocatalyst, film catalyst or magnetically separable photocatalyst has been attempted to circumvent the difficulty in catalyst recovery associated with powdered catalyst [7–10], whereas the advantage in the separation of the specific photocatalysts is generally achieved at the expense of photocatalytic activity [6,11].

Elongated TiO_2 nanoparticles synthesized via an alkaline hydrothermal route have attracted great attention due to its high specific surface area and large aspect ratio [12–14]. In addition, TiO_2 nanoparticles with high aspect ratio exhibit prominent advantages in the sedimentation process over powdered catalysts, effectively facilitating solid–liquid separation and catalyst recovery [15–18]. It is noteworthy that the structures of the elongated TiO_2 nanoparticles vary with the synthesis methods and post-treatments, which may substantially impact their photocatalytic activities. In general, as-synthesized TiO_2 nanoparticles in titanate form show relatively low photocatalytic activities for pollutant degradation [18–20]. Modification of as-synthesized TiO_2 nanoparticles by calcination may enhance their photocatalytic activity. For example, Yu et al. [21] modified TiO_2 nanotube using calcination and found that the photocatalytic activity of the modified TiO_2 nanotube for acetone oxidation in air was closely linked to the calcination temperature. Alternatively, the structures of TiO_2 nanoparticles as well as their photocatalytic behaviors can be tuned via the hydrothermal post-treatment. Zhu et al. [15] converted titanate nanofiber into anatase nanofiber using a hydrothermal reaction and observed the substantially enhanced photocatalytic activity of anatase nanofiber for the degradation of sulforhodamine dye as compared to titanate

* Corresponding author. Tel.: +86 25 83595831; fax: +86 25 83707304.
E-mail address: srzheng@nju.edu.cn (S. Zheng).

0304-3894/$ – see front matter © 2009 Elsevier B.V. All rights reserved.
doi:10.1016/j.jhazmat.2009.11.057

nanofiber. In parallel, Yu and Xu [17] synthesized anatase TiO_2 nanorods by the hydrothermal conversion of TiO_2 nanofibers in acid solution and observed a higher photocatalytic activity for aqueous Rhodamine B dye as compared to P25.

It should be pointed out that the previous studies on the catalytic behaviors of elongated TiO_2 nanoparticles mainly focused on the photocatalytic degradation of organic pollutants via an oxidation mechanism. To our best knowledge, however, the properties of TiO_2 nanoparticles for photocatalytic reduction have been seldom addressed. In this study, TiO_2 nanofiber was prepared using the alkaline hydrothermal method and the structures of TiO_2 nanoparticles were tuned using either thermal or hydrothermal post-treatments. Photocatalytic phenol degradation and Cr(VI) reduction over the catalysts were investigated to systematically evaluate the impacts of their structural properties on the catalytic behaviors for photocatalytic oxidation and reduction. For comparison purpose, Degussa P25, a commercially available TiO_2 consisting of 80% anatase and 20% rutile, was also tested as a reference catalyst for photocatalytic phenol degradation and Cr(VI) reduction.

2. Experimental

2.1. Catalyst preparation

All chemicals were of analytical grade and were used without further purification. TiO_2 nanofiber was synthesized using the alkaline hydrothermal method and other TiO_2 nanoparticles with varied structural properties were prepared using different post-treatments with the as-prepared TiO_2 nanofiber as the precursor. For the preparation of TiO_2 nanofiber, 4 g TiO_2 powder (P25, Degussa) was added into 80 ml of 15 M NaOH solution and the suspension system was further stirred at room temperature for 2 h. The mixture was then transferred to a Teflon-lined stainless autoclave which was heated at 150 °C for 48 h. The precipitate was recovered by filtration, followed by repeated washing with distilled water. The solid particles were again suspended in 200 ml of distilled water with solution pH adjusted to 4.0 using 0.1 M HNO_3 solution, and the mixture was further stirred for 8 h. The resulting TiO_2 nanofiber, denoted as TiO_2-NF, was dried at 80 °C for 10 h. Different TiO_2 nanoparticles were prepared by treating the as-synthesized TiO_2-NF using either calcination or hydrothermal reaction. For thermal post-treatment, as-synthesized TiO_2-NF was calcined at 400 or 600 °C for 4 h. The resultant TiO_2 nanoparticles are referred to as TiO_2-NF-*X*, where *X* denotes the calcination temperature (°C). For hydrothermal treatment, 2.0 g of as-synthesized TiO_2-NF was added into 80 ml of distilled water and the solution pH was adjusted to 2.0 using 0.1 M HNO_3 solution. The mixture was transferred into a Teflon-lined stainless autoclave, which was subjected to hydrothermal treatment at 175 °C for 48 h. The solid particles were recovered by filtration, followed by repeated washing by distilled water and drying at 80 °C for 10 h. The resultant TiO_2 nanoparticle is designated to TiO_2-NF-H.

2.2. Material characterization

X-ray diffraction (XRD) patterns were collected in a Rigaku D/max-RA powder diffraction-meter using Cu K_α radiation. Transmission electron microscopy (TEM) images of the samples were collected on a Hitachi H-800 transmission electron microscope. The specific surface areas of the samples were determined by N_2 adsorption at −196 °C (77 K) on a Micrometrics ASAP 2020 apparatus. The Raman spectra of the samples were recorded on the JY HR-800 instrument. The UV–vis spectra of the samples were obtained in SHIMAD UV-2401PC UV/vis spectrometer using $BaSO_4$ as a reference. The surface zeta potentials (ζ) of the samples were measured using a Zeta Potential Analyzer (Zeta PALS, Brookhaven Instruments Co.). Typically, 10 mg of the samples were dispersed in 100 ml of distilled water with varied pH and were equilibrated for 24 h prior to zeta potential measurements.

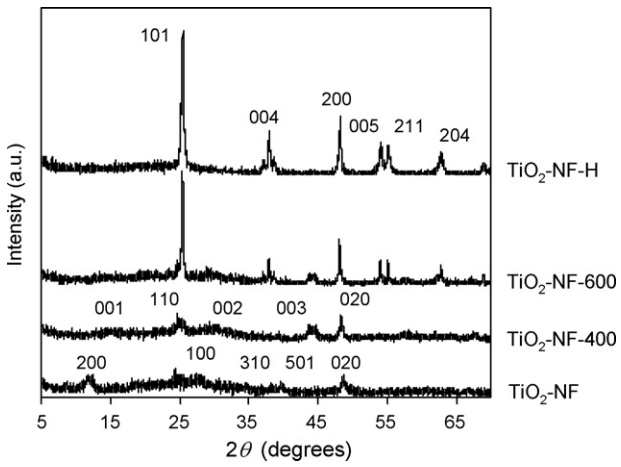

Fig. 1. XRD patterns of TiO_2 nanoparticles.

2.3. Photocatalytic reactions

Photocatalytic reactions were conducted in a commercial NDC photo-reactor equipped with a 500 ml cylindrical Pyrex vessel irradiated directly by a high pressure mercury lamp (125 W), which was described in Figure S1 (see Supporting information). For photocatalytic phenol degradation, 0.2 g of the catalyst was mixed with 500 ml of 50 mg l^{-1} phenol solution which was further stirred in the dark for 60 min to reach the adsorption equilibrium prior to the photocatalytic test. During the photocatalytic reaction, samples were collected at selected time intervals and the catalyst particles were removed by centrifugation. The residual phenol concentration was determined using HPLC (Agilent 1200, USA), equipped with an ultraviolet (UV) detector and a C18 reversed phase column (250 mm × 4.5 mm, 5 μm, Agilent, USA) at 30 °C. The mobile phase consists of water and acetonitrile (40/60, v/v) with a flow rate of 1.0 ml min^{-1}.

As for photocatalytic Cr(VI) reduction, 0.5 g of the catalyst was suspended in 500 ml of 40 mg l^{-1} Cr(VI) solution with solution pH 2.5 adjusted using 1.0 M H_2SO_4. The suspension was further stirred in the dark for 60 min. During the photo-reaction, samples were collected at preset time intervals. The catalyst powders were removed by filtration and the residual Cr(VI) concentration was determined spectrophotometrically using diphenylcarbazide as the color agent.

3. Results and discussion

3.1. Material characterization

The XRD patterns of the catalysts are compared in Fig. 1. For TiO_2 nanofiber, weak diffraction peaks were observed with 2θ at 12.4°, 28.4°, 40.1° and 48.7°, attributed to monoclinic titanate $H_2Ti_3O_7{\cdot}xH_2O$ [22,23]. The generation of titanate under alkaline hydrothermal conditions is based on a dissolution–recrystallization mechanism, by which TiO_2 precursor is irreversibly converted into soluble titanate species and these species are further thermodynamically deposited and crystallized into lamellar titanate [24,25]. Upon calcination of as-synthesized TiO_2 nanofiber at 400 °C for 4 h, new diffraction peaks were observed at 25.4°, 30.3°, 44.3° and 48.4°, assigned to metastable polymorph TiO_2-B [26,27]. This conversion could be ascribed to the dehydration and recrystallization

of layered titanate during the calcination process [12,28]. Further increasing the calcination temperature from 400 to 600 °C led to the emergence of new diffraction peaks, attributed to anatase TiO_2. It is noteworthy that the diffraction peaks characteristic of TiO_2-B still visible in the XRD pattern of TiO_2-NF-600, suggesting that TiO_2-NF-600 virtually consists of both TiO_2-B and anatase phases. In contrast, much different XRD pattern was observed upon hydrothermal post-treatment of as-synthesized TiO_2 nanofiber. As shown in Fig. 1, the diffraction peaks characteristic of typical anatase TiO_2 were identified. Moreover, other diffraction peaks characteristic of titanate, TiO_2-B and rutile were not observed, indicative of the presence of pure anatase TiO_2 crystalline phase. The crystalline conversion of titanate into anatase is generally ascribed to a topochemical reaction process, by which titanate is dehydrated under acidic conditions and in-situ converted into anatase with retention of its pristine morphology [16].

The crystalline phase transformation resulting from different post-treatments was also confirmed by Raman analysis. The Raman spectra of TiO_2 nanoparticles are presented in Fig. 2. For TiO_2-NF, the bands characteristic of titanium and oxygen stretching vibration in the TiO_6 octahedra were observed at 157.3, 190.8, 264.3, 361.4, 421.6, 457.5, 592.9 and 673.3 cm^{-1}, which are in good agreement with the Raman spectrum of $H_2Ti_3O_7$ obtained by Kolen'ko et al. [29]. Calcination of TiO_2-NF led to the disappearance of Raman peaks characteristic of titanate in concomitance of the presence of new Raman peaks at 160.8, 187.3, 413.4, 464.4 and 646.6 cm^{-1}, assigned to metastable TiO_2-B [27]. Further increasing the calcination temperature to 600 °C resulted in new Raman peaks at 144.9,

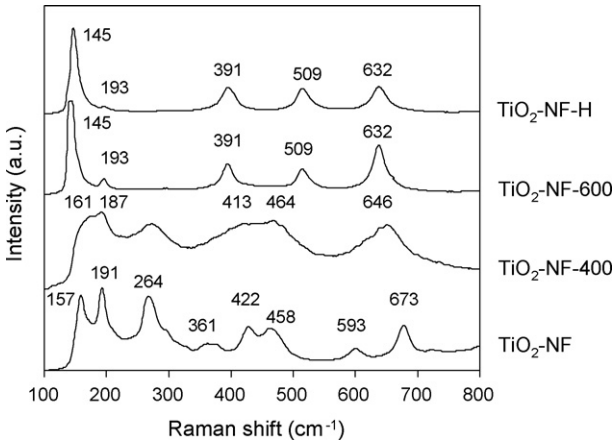

Fig. 2. Raman spectra of TiO_2 nanoparticles.

192.8, 390.7, 508.6 and 631.6 cm^{-1}, assigned to the active modes of typical anatase TiO_2 [30,31], suggesting the presence of anatase phase. For TiO_2-NF-H, similar Raman peaks characteristic of anatase TiO_2 were observed to that of TiO_2-NF-600, further indicating that TiO_2-NF-H consists of pure anatase phase.

The morphologies of TiO_2 nanoparticles can be clearly visualized using TEM and their TEM images are shown in Fig. 3. For as-synthesized TiO_2-NF, flexible TiO_2 nanofibers with diameters ranging from about 20–50 nm and length of several microm-

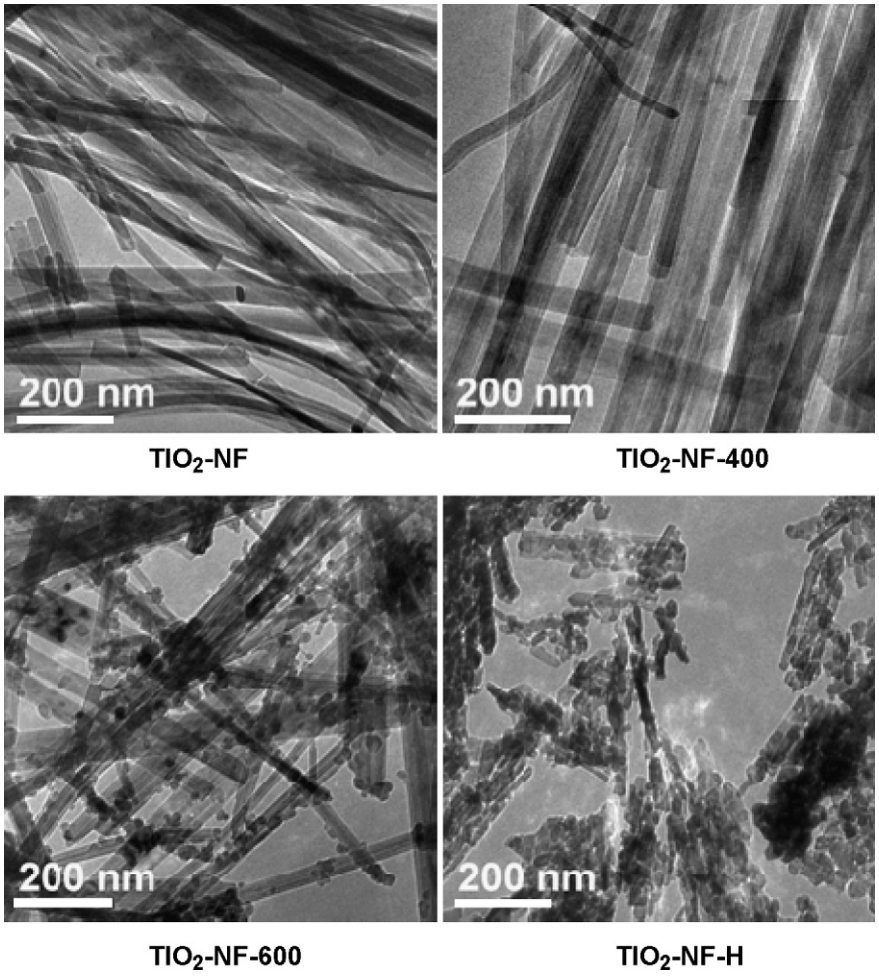

Fig. 3. TEM images of TiO_2 nanoparticles.

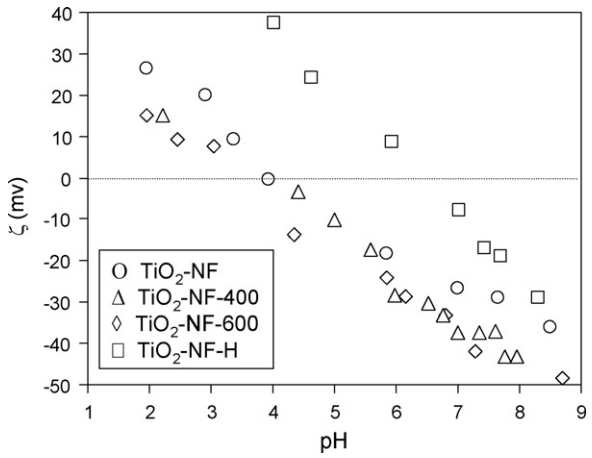

Fig. 4. Surface charge density (ζ) versus solution pH for different TiO_2 nanoparticles.

eters can be clearly observed, resulting from the fast growth of nanosheets under alkaline hydrothermal conditions [32]. For TiO_2-NF-400, minor changes were observed in comparison with as-synthesized TiO_2-NF. At calcination temperature of 600 °C, the TEM image of TiO_2-NF-600 displays rod-like morphology with markedly decreased diameters and the nanorods were decorated with a large amount of nanoparticles with diameters of about 10–20 nm, due to dehydrolyzation and crystallization of a fraction of titanate on the nanofiber surface. XRD results show that TiO_2-NF-600 consists of both TiO_2-B and anatase phases and TiO_2-NF-400 is composed of pure TiO_2-B. Therefore, it is speculated that the particles and nanorods consist of anatase and TiO_2-B, respectively. The TEM image of TiO_2-NF-H shows that the morphology of TiO_2-NF-H is much different from those obtained from thermal post-treatment. TiO_2-NF-H are intrinsically composed of nanoparticles with diameters around 10–20 nm which further aggregate into nanofibers.

Zeta potentials (ζ) of the nanoparticles as a function of solution pH is compiled in Fig. 4 and the obtained values of isoelectric points (IEPs) of the nanoparticles are listed in Table 1. For all TiO_2 nanoparticles, the surface charge densities monotonically decreased with the increase of solution pH. The IEPs were estimated to be 4.0, 4.0 and 3.9 for TiO_2-NF, TiO_2-NF-400 and TiO_2-NF-600, respectively. The identical IEP of TiO_2-NF-400 to that of TiO_2-NF reflects the similar nature of surface hydroxyl group of TiO_2-B to that of titanate. In addition, the similar IEP of TiO_2-NF-600 to TiO_2-NF-400 suggests that the surface of TiO_2-NF-600 is dominated by surface hydroxyl groups from TiO_2-B instead of anatase TiO_2 in TiO_2-NF-600 due to the substantially high IEP of anatase TiO_2 [33]. The IEP of TiO_2-NF-H was found to be about 6.5, identical to that of anatase [33].

The results of N_2 adsorption analysis are listed in Table 1. BET surface area of TiO_2-NF was found to be 55.6 $m^2\,g^{-1}$. Calcination at 400 °C led to a slight decrease in BET surface area of TiO_2-NF-400, whereas further increasing the calcination temperature to 600 °C resulted in a sharp decrease of BET surface area to 24.6 $m^2\,g^{-1}$, probably due to the transformation of a fraction of TiO_2 nanofiber into TiO_2 nanoparticles. For TiO_2-NF-H, BET surface area is 44.9 $m^2\,g^{-1}$, slightly lower than those of TiO_2-NF and TiO_2-NF-400.

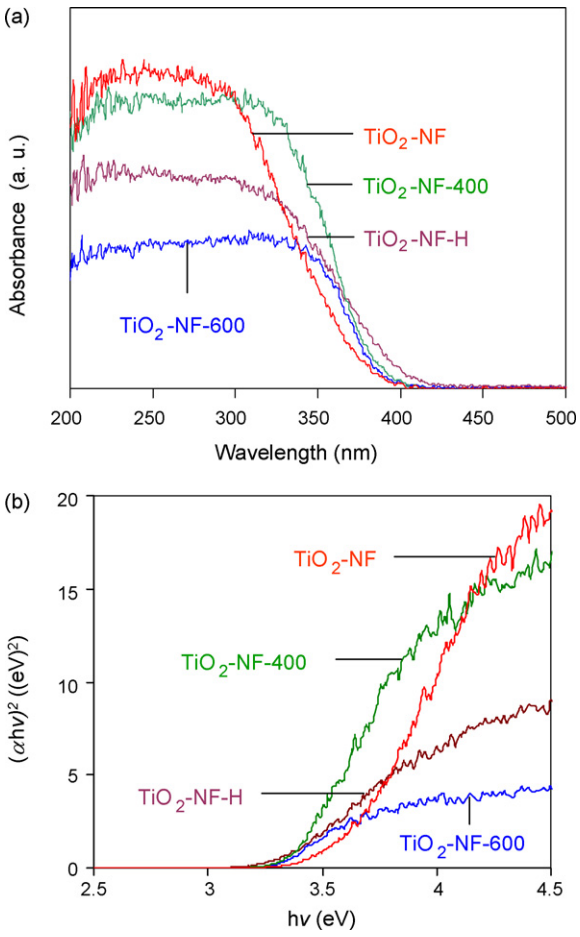

Fig. 5. (a) UV–vis spectra and (b) plots of $(\alpha h\nu)^2$ versus $h\nu$ of the catalysts.

The UV–vis absorption spectra of the catalysts are shown in Fig. 5a. The absorption threshold of TiO_2-NF was slightly blue shifted, indicative of a larger band gap of TiO_2-NF as compared to other catalysts. For a direct semiconductor, the optical absorbance can be described using equation 1 [34]:

$$\alpha h\nu = B(h\nu - E_g)^{1/2} \quad (1)$$

where α is the absorbance intensity at light frequency of ν, B the absorbance constant and E_g the band gap energy, respectively.

The plots of $(\alpha h\nu)^2$ versus $h\nu$ are compared in Fig. 5b. E_g is the intercept of linear extrapolation to $h\nu$ axis and the obtained band gap energies for TiO_2-NF, TiO_2-NF-400, TiO_2-NF-600 and TiO_2-NF-H are found to be 3.60, 3.37, 3.32 and 3.24 eV, respectively, suggesting a considerably larger band gap of TiO_2-NF as compared to other TiO_2 nanoparticles tested in this study.

3.2. Photocatalytic phenol degradation

The photocatalytic degradation of aqueous phenol over the catalysts is compiled in Fig. 6. For phenol degradation over all photocatalysts, aqueous phenol concentration continuously dimin-

Table 1
Structural properties of TiO_2 nanoparticles.

Sample	Crystalline phase composition	BET ($m^2\,g^{-1}$)	IEP	Band gap (eV)
TiO_2-NF	Titanate	55.6	4.0	3.60
TiO_2-NF-400	TiO_2-B	52.0	4.0	3.37
TiO_2-NF-600	TiO_2-B + anatase	24.6	3.9	3.32
TiO_2-NF-H	Anatase	44.9	6.5	3.24

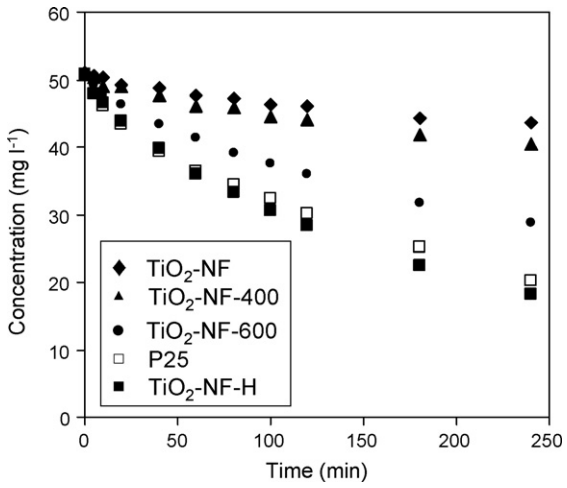

Fig. 6. Photocatalytic phenol degradation over TiO_2 nanoparticles.

ished with UV irradiation, indicating that the synthesized TiO_2 nanoparticles are effective photocatalysts. However, phenol degradation efficiency varied with the structural properties of the catalysts. After UV irradiation for 240 min, phenol removal were found to be 14.7%, 20.3%, 42.9%, 64.2% and 60.2% for TiO_2-NF, TiO_2-NF-400, TiO_2-NF-600, TiO_2-NF-H and P25, reflecting the highest photocatalytic activity of TiO_2-NF-H among the catalysts examined. As for degradation kinetics, the fitting results showed that phenol degradation over the photocatalysts could be well described using first-order kinetics:

$$r = -\frac{dC_t}{dt} = kC_t \quad (2)$$

$$\ln\left(\frac{C_0}{C_t}\right) = kt \quad (3)$$

where r is the reaction rate, C_t the concentration of aqueous phenol at reaction time t, C_0 the initial phenol concentration and k the reaction rate constant.

The fitting parameters of phenol degradation kinetics are listed in Table 2. The rate constants of photocatalytic phenol degradation were calculated to be 7.7×10^{-4}, 9.4×10^{-4}, 2.3×10^{-3}, 4.2×10^{-3} and 3.6×10^{-3} mg l^{-1} min^{-1} for TiO_2-NF, TiO_2-NF-400, TiO_2-NF-600, TiO_2-NF-H and P25, respectively, indicative of an increasing catalytic activity order of TiO_2-NF < TiO_2-NF-400 < TiO_2-NF-600 < P25 < TiO_2-NF-H.

In principle, the photocatalytic activity is closely linked to the structural properties of the photocatalyst, such as crystallinity, crystalline phase composition and specific surface area. Because BET surface area of TiO_2-NF is approximately identical to that TiO_2-NF-400, the higher phenol degradation rate of TiO_2-NF-400 compared to TiO2-NF is attributed to the lower photocatalytic activity of its titanate structure [18–20]. Furthermore, the band gap of TiO_2-NF was found to be 3.60 eV, substantially larger than other catalysts. The larger band gap of TiO_2-NF leads to less effective absorption of excitation light, also giving rise to the low photocatalytic activity. Although the specific surface areas of TiO_2-NF-400 and TiO_2-NF are about two times as large as TiO_2-NF-600, substantially higher phenol degradation rate was observed for TiO_2-NF-600 than TiO_2-NF-400 and TiO_2-NF, suggesting that the higher phenol degradation efficiency of TiO_2-NF-600 results from the different crystalline phase composition of TiO_2-NF-600. In general, TiO_2 consisting of anatase exhibits higher photocatalytic activity as compared to TiO_2 with other crystalline phases [3–5]. Moreover, semiconductor containing mixed crystalline phases may show higher photocatalytic activity as a result of the enhanced separation and effective inhabitation of recombination of excited electrons and holes [35,36]. Note that TiO_2-NF-600 consists of both TiO_2-B and anatase. In comparison with TiO_2-NF-400, therefore, the higher photocatalytic activity of TiO_2-NF-600 for phenol degradation can be attributed to either the presence of anatase or to the specific crystalline composition of mixed TiO_2-B and anatase.

As for TiO_2-NF-H, the phenol degradation was further enhanced in comparison with other catalysts tested. It should be pointed out that phenol degradation over TiO_2-NF-H is even faster than that over P25, a commercially available TiO_2 consisting of mixed anatase and rutile. Similarly, higher photocatalytic activities of TiO_2 nanoparticles prepared hydrothermally using TiO_2 nanotube as the precursor were also observed as compared to P25 [18–20]. Yu et al. [37] studied the photocatalytic acetone oxidation over TiO_2 nanofiber prepared from hydrothermal post-treatment of TiO_2 nanotube and attributed the enhanced activity to its smaller crystallite size, larger specific surface area, and higher pore volume. For TiO_2-NF-H, however, its BET surface area is approximately identical to those of P25, TiO_2-NF and TiO_2-NF-400, suggesting that other structural factors of TiO_2-NF-H account for the enhanced photocatalytic activity for phenol degradation. It is noteworthy that surface hydroxyl groups of TiO_2 are believed to be favorable for the generation of the highly active hydroxyl radical beneficial for oxidative degradation of organic compounds [38,39]. In contrast to other TiO_2 nanoparticles obtained using thermal post-treatment, TiO_2 nanoparticle prepared by the hydrothermal route is generally abundant in surface hydroxyl groups [20,40], which facilitates the generation of hydroxyl radical upon UV irradiation and eventually enhances phenol degradation.

For a heterogeneous photocatalytic system, in principle, the reaction presumably occurs on the catalyst surface. Therefore, reactant adsorption on catalyst surface is believed to be a prerequisite step and the photocatalytic reaction generally follows the Langmuir–Hinshelwood model. In order to verify the photocatalytic mechanism of phenol degradation over TiO_2-NF-H, the influence of initial phenol concentration on the initial degradation rate was conducted and the results are shown in Fig. 7. As shown in Fig. 7a, phenol degradation rate fast increased and then gently augmented with the increase of initial phenol concentration. The dependence of phenol degradation rate on the initial concentration was fitted according to the Langmuir–Hinshelwood model,

$$r_0 = -\frac{dC_0}{dt} = -k\frac{bC_0}{1 + bC_0} \quad (4)$$

$$\frac{1}{r_0} = \frac{1}{kb}\frac{1}{C_0} + \frac{1}{k} \quad (5)$$

Table 2
Rate constants of photocatalytic phenol degradation and Cr(VI) reduction.

Sample	Phenol degradation (mg l^{-1} min^{-1})	R^2	Cr(VI) reduction (mg l^{-1} min^{-1})	R^2
TiO_2-NF	7.7×10^{-4}	0.97	2.3×10^{-3}	0.98
TiO_2-NF-400	9.4×10^{-4}	0.97	1.5×10^{-3}	0.97
TiO_2-NF-600	2.3×10^{-3}	0.98	1.6×10^{-3}	0.98
TiO_2-NF-H	4.2×10^{-3}	0.99	7.3×10^{-3}	0.98
P25	3.6×10^{-3}	0.98	1.1×10^{-2}	0.97

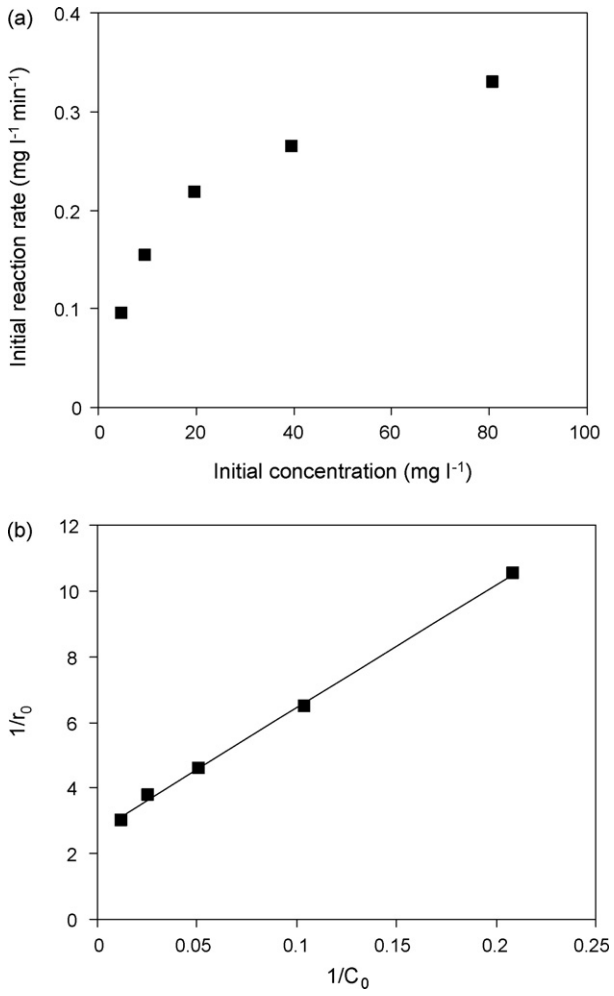

Fig. 7. (a) Dependence of initial phenol degradation rate on initial phenol concentration and (b) linear plot of $1/r_0$ versus $1/C_0$.

where r_0 is the initial phenol degradation rate at initial concentration C_0, k the reaction rate constant and b the equilibrium constant for reactant adsorption on TiO_2 surface.

The plot of $1/r_0$ values versus $1/C_0$ is shown in Fig. 7b. The linear plot of $1/r_0$ versus $1/C_0$ with R^2 higher than 0.99 suggests that phenol degradation over TiO_2-NF-H can be well described using Langmuir–Hinshelwood model, reflecting that phenol degradation over TiO_2-NF-H is controlled by phenol pre-adsorption.

3.3. Photocatalytic Cr(VI) reduction

Besides photocatalytic phenol degradation, photocatalytic reduction of aqueous Cr(VI) was also preformed to evaluate the catalytic activities of TiO_2 nanoparticles. In the presence of photocatalyst, Cr(VI) can be reduced to Cr(III) by the excited electrons upon UV irradiation and the overall reaction of photocatalytic Cr(VI) reduction could be described as follows [41,42]:

$$Cr_2O_7^{2-} + 14H^+ + 6e^- \rightarrow 2Cr^{3+} + 7H_2O \quad (6)$$

$$2H_2O + 4h^+ \rightarrow O_2 + 4H^+ \quad (7)$$

Photocatalytic Cr(VI) reduction over the examined catalysts at pH 2.5 are compiled in Fig. 8. After reaction for 180 min, aqueous Cr(VI) was removed by about 32%, 23%, 26%, 75% and 88% for TiO_2-NF, TiO_2-NF-400, TiO_2-NF-600, TiO_2-NF-H and P25, respectively. Similarly, the photocatalytic Cr(VI) reduction could be well described using first-order kinetics and the fitting results are listed

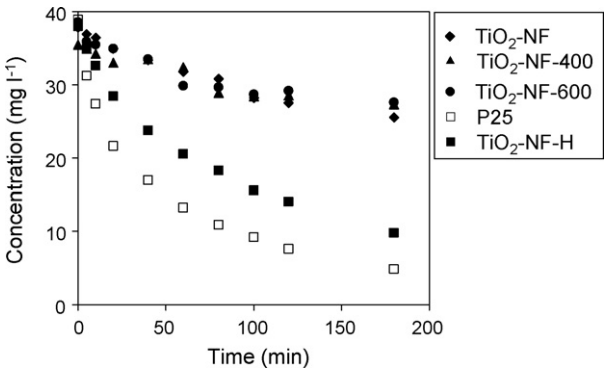

Fig. 8. Photocatalytic Cr(VI) reduction over TiO_2 nanoparticles.

in Table 2. The photocatalytic Cr(VI) reduction rate constants were calculated to be 2.3×10^{-3}, 1.5×10^{-3}, 1.6×10^{-3}, 7.3×10^{-3} and 1.1×10^{-2} mg l^{-1} min^{-1} for TiO_2-NF, TiO_2-NF-400, TiO_2-NF-600, TiO_2-NF-H, reflecting an increasing catalytic activity order of TiO_2-NF-400 ~ TiO_2-NF-600 < TiO_2-NF < TiO_2-NF-H < P25. Note that the photocatalytic activity of TiO_2-NF is found to be higher than those of TiO_2-NF-400 and TiO_2-NF-600, and the Cr(VI) reduction rate constant of P25 is higher as compared to that of TiO_2-NF-H, which is in contrast to the catalytic activity trend of photocatalytic phenol degradation.

For photocatalytic Cr(VI) reduction, Cr(VI) reduction efficiency is found to be pH dependent and a higher Cr(VI) removal can be

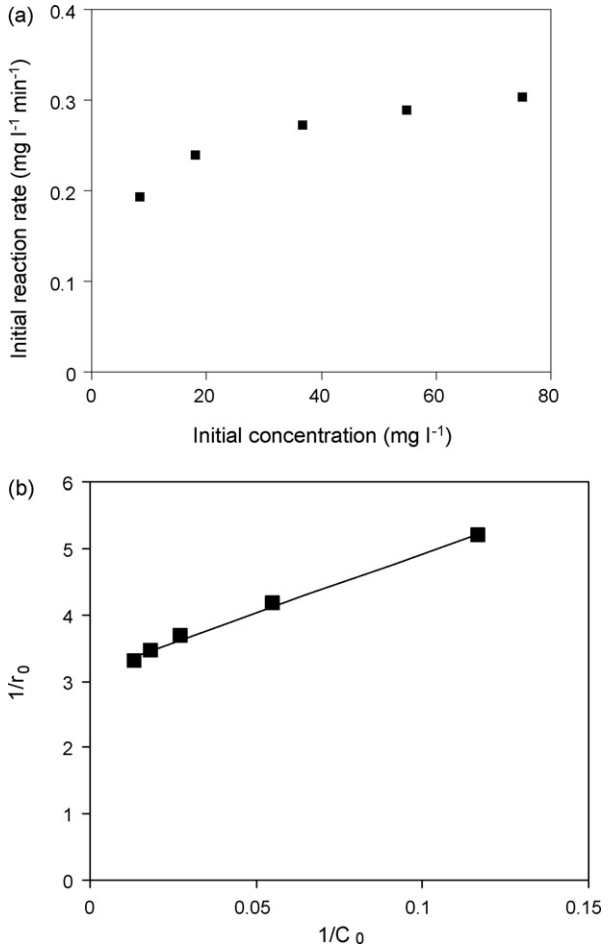

Fig. 9. (a) Dependence of initial Cr(VI) reduction rate on initial Cr(VI) concentration and (b) linear plot of $1/r_0$ versus $1/C_0$.

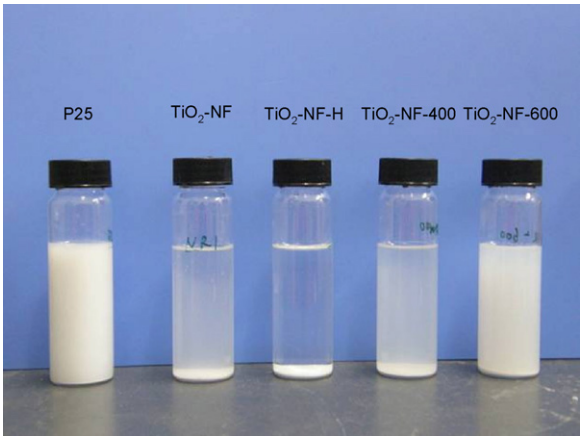

Fig. 10. Sedimentation properties of TiO_2 nanoparticles.

generally achieved at lower solution pH because the potential of CrO_4^{2-}/Cr^{3+} pair decreases by 98 mV per pH unit with the increase of solution pH [43]. Therefore, the presence of acid sites on catalyst surface may favor Cr(VI) reduction. For example, Jiang et al. [44] compared the catalytic activities of alkaline treated sulfated TiO_2 and sulfated TiO_2 for photocatalytic Cr(VI) reduction and observed considerably higher photocatalytic activity of sulfated TiO_2 as compared to alkaline treated sulfated TiO_2 due to the decreased surface acidity of alkaline treated TiO_2. For titanate, Zheng et al. [45] studied the surface acidity of acid exchanged titanate using microcalorimetry with NH_3 as the probe molecule and detected a large amount of acid sites with varied acid strength. In parallel, TiO_2 nanotube was found to be active for the hydrolysis of 2-chlorethyl ethylsulfide due to the presence of surface acid sites [46]. Therefore, the considerably higher catalytic activity of TiO_2-NF than those of TiO_2-NF-400 and TiO_2-NF-600 can be attributed to the presence of surface acidity of TiO_2-NF although TiO_2-NF responses to relatively narrow irradiation light due to its large band gap and titanate is less active crystalline phase as indicated by photocatalytic phenol degradation. In comparison with TiO_2-NF-400, TiO_2-NF-600 shows a higher activity for phenol degradation, but comparable activity for Cr(VI) reduction, implying the more predominant impact of surface area than that of crystalline phase on photocatalytic Cr(VI) reduction. As for TiO_2-NF-H, it is understandable that similar to phenol degradation the highest catalytic activity for photocatalytic Cr(VI) reduction is achieved over TiO_2-NF-H among the examined nanofibers due to its anatase phase, comparable specific surface area with TiO_2-NF and TiO_2-NF-400, and considerable larger specific surface area than TiO_2-NF-600. It should be pointed out that in contrast to phenol degradation TiO_2-NF-H shows a lower catalytic activity for Cr(VI) reduction as compared to P25. For phenol degradation, the high surface hydroxyl group concentration accounts for the high catalytic activity of TiO_2-NF-H. Photocatalytic Cr(VI) reduction, however, is mediated by excited electrons instead of hydroxyl radicals. Therefore, the mixed anatase and rutile phase of P25 leads to its higher catalytic activity than TiO_2-NF-H for Cr(VI) reduction.

Similar to photocatalytic phenol degradation, photocatalytic Cr(VI) reduction also occurs on the surface of the photocatalyst, assumed to follow the Langmuir–Hinshelwood model. The influence of initial Cr(V) concentration on initial reaction rate was conducted and the results are shown in Fig. 9. The results were fitted according to equation 5. As shown in Fig. 9b, the linear plot of $1/r_0$ versus $1/C_0$ indicates that the photocatalytic Cr(VI) reduction can also be described using the Langmuir–Hinshelwood model, reflecting a surface adsorption controlled reaction mechanism.

The prominent advantages of TiO_2 nanoparticles with high aspect ratio are their excellent sedimentation properties. For the tested TiO_2 nanoparticles, the sedimentation properties were preliminarily compared by suspending 25 mg of catalyst in 30 ml distilled water under stirring, followed by static sedimentation for 30 min and the results are shown in Fig. 10. Compared with P25, all synthesized catalysts were fast precipitated. Furthermore, TiO_2-NF-H exhibits the best sedimentation efficiency among the examined catalysts.

4. Conclusions

In this study, TiO_2 nanofiber was prepared via an alkaline hydrothermal reaction and TiO_2 nanoparticles with varied structural properties were obtained using thermal and hydrothermal post-treatments. Characterization results show that the crystalline phase of TiO_2-NF is titanate in nature. Thermal treatment of TiO_2-NF leads to the transformation of titanate to TiO_2-B at 400 °C and to mixed TiO_2-B and anatase at 600 °C, whereas pure anatase can be obtained using hydrothermal post-treatment. For photocatalytic phenol degradation, TiO_2-NF exhibits a low catalytic activity compared with the post-treated catalysts. In addition, the presence of mixed TiO_2-B and anatase in TiO_2-NF-600 considerably enhances phenol degradation. TiO_2-NF-H shows a higher catalytic activity than that of P25 due to its high concentration of surface hydroxyl groups. In contrast to photocatalytic phenol degradation, TiO_2-NF shows a higher catalytic activity as compared to TiO_2-NF-400 and TiO_2-NF-600 for photocatalytic Cr(VI) reduction, attributed to the presence of surface acidity in TiO_2-NF. The approximately identical catalytic activity of TiO_2-NF-400 to that of TiO_2-NF-600 suggests a more prominent impact of specific surface area on Cr(VI) reduction than that of crystalline phase composition. Because photocatalytic Cr(VI) reduction is mediated by excited electrons, TiO_2-NF-H has a relatively lower catalytic activity as compared to P25 for photocatalytic Cr(V) reduction.

Acknowledgements

This work was supported by the National Natural Science Foundation of China (Nos. 20677026 and 20877039) and Scientific and Technical Programs of China (2008ZX07421-006 and 2006BAJ08B02).

Appendix A. Supplementary data

Supplementary data associated with this article can be found, in the online version, at doi:10.1016/j.jhazmat.2009.11.057.

References

[1] A. Fujishima, K. Honda, Electrochemical photolysis of water at a semiconductor electrode, Nature 238 (1972) 37–38.
[2] S.N. Frank, A.J. Bard, Heterogeneous photocatalytic oxidation of cyanide ion in aqueous solutions of titanium dioxide powder, J. Am. Chem. Soc. 99 (1977) 303–305.
[3] M.R. Hoffmann, S.T. Martin, W. Choi, D.W. Bahnemann, Environmental applications of semiconductor photocatalysis, Chem. Rev. 95 (1995) 69–96.
[4] A.L. Linsebigler, G. Lu, J.T. Yates Jr., Photocatalysis on TiO_2 surfaces: principles, mechanisms, and selected results, Chem. Rev. 95 (1995) 735–758.
[5] A. Fujishima, T.N. Rao, D.A. Tryk, Titanium dioxide photocatalysis, J. Photochem. Photobiol. C 1 (2000) 1–21.
[6] D. Beydoun, R. Amal, G.K.C. Low, S. Mc Evoy, Novel photocatalyst: titania-coated magnetite. Activity and photodissolution, J. Phys. Chem. B 104 (2000) 4387–4396.
[7] P.F. Fu, Y. Luan, X.G. Dai, Preparation of activated carbon fibers supported TiO_2 photocatalyst and evaluation of its photocatalytic reactivity, J. Mol. Catal. A: Chem. 221 (2004) 81–88.
[8] R.L. Pozzo, M. Baltanas, A. Cassano, Supported titanium oxide as photocatalyst in water decontamination: state of the art, Catal. Today 39 (1997) 219–231.
[9] N.B. Jackson, C.W. Wang, Z. Luo, J. Schwitzgebel, J.G. Ekerdt, J.R. Brock, A. Heller, Attachment of TiO_2 powders to hollow glass microbeads: activity of the TiO_2-coated beads in the photo-assisted oxidation of ethanol to acetaldehyde, J. Electrochem. Sci. 138 (1991) 3660–3664.

[10] D. Beydoun, R. Amal, G. Low, S. McEvoy, Occurrence and prevention of photodissolution at the phase junction of magnetite and titanium dioxide, J. Mol. Catal. A: Chem. 180 (2002) 193–200.
[11] V. Belessi, D. Lambropoulou, I. Konstantinou, R. Zboril, J. Tucek, D. Jancik, T. Albanis, D. Petridis, Structure and photocatalytic performance of magnetically separable titania photocatalysts for the degradation of propachlor, Appl. Catal. B: Environ. 87 (2009) 181–189.
[12] T. Kasuga, M. Hiramatsu, A. Hoson, T. Sekino, K. Niihara, Formation of titanium oxide nanotube, Langmuir 14 (1998) 3160–3163.
[13] D.V. Bavykin, F.C. Walsh, Elongated titanate nanostructures and their applications, Eur. J. Inorg. Chem. (2009) 977–997.
[14] D.V. Bavykin, J.M. Friedrich, F.C. Walsh, Protonated titanates and TiO_2 nanostructured materials: synthesis, properties, and applications, Adv. Mater. 18 (2006) 2807–2824.
[15] H.Y. Zhu, X.P. Gao, Y. Lan, D.Y. Song, Y.X. Xi, J.C. Zhao, Hydrogen titanate nanofibers covered with anatase nanocrystals: A delicate structure achieved by the wet chemistry reaction of the titanate nanofibers, J. Am. Chem. Soc. 126 (2004) 8380–8381.
[16] H.Y. Zhu, Y. Lan, X.P. Gao, S.P. Ringer, Z.F. Zheng, D.Y. Song, J.C. Zhao, Phase transition between nanostructures of titanate and titanium dioxides via simple wet-chemical reactions, J. Am. Chem. Soc. 127 (2005) 6730–6736.
[17] Y. Yu, D. Xu, Single-crystalline TiO_2 nanorods: highly active and easily recycled photocatalysts, Appl. Catal. B: Environ. 73 (2007) 166–171.
[18] L.L. Costa, A.G.S. Prado, TiO_2 nanotubes as recyclable catalyst for efficient photocatalytic degradation of indigo carmine dye, J. Photochem. Photobiol. A: Chem. 201 (2009) 45–49.
[19] H.H. Ou, C.H. Liao, Y.H. Liou, J.H. Hong, S.L. Lo, Photocatalytic oxidation of aqueous ammonia over microwave-induced titanate nanotubes, Environ. Sci. Technol. 42 (2008) 4507–4512.
[20] G.S. Guo, C.N. He, Z.H. Wang, F.B. Gu, D.M. Han, Synthesis of titania and titanate nanomaterials and their application in environmental analytical chemistry, Talanta 72 (2007) 1687–1692.
[21] J.G. Yu, H.G. Yu, B. Cheng, C. Trapalis, Effects of calcination temperature on the microstructures and photocatalytic activity of titanate nanotubes, J. Mol. Catal. A: Chem. 249 (2006) 135–142.
[22] C.H. Lin, J.H. Chao, C.H. Liu, J.C. Chang, F.C. Wang, Effect of calcination temperature on the structure of a Pt/TiO_2 (B) nanofiber and its photocatalytic activity in generating H_2, Langmuir 24 (2008) 9907–9915.
[23] C.C. Tsai, H. Teng, Structural features of nanotubes synthesized from NaOH treatment on TiO_2 with different post-treatments, Chem. Mater. 18 (2006) 367–373.
[24] E. Morgado Jr., M.A.S. de Abreu, G.T. Moure, B.A. Marinkovic, P.M. Jardim, A.S. Araujo, Characterization of nanostructured titanates obtained by alkali treatment of TiO2-anatases with distinct crystal sizes, Chem. Mater. 19 (2007) 665–676.
[25] D. Wu, J. Liu, X.N. Zhao, A.D. Li, Y.F. Chen, N.B. Ming, Sequence of events for the formation of titanate nanotubes, nanofibers, nanowires, and nanobelts, Chem. Mater. 18 (2006) 547–553.
[26] T.P. Feist, S.J. Mocarski, P.K. Davies, A.J. Jacobson, J.T. Lewandowski, Formation of TiO_2(B) by proton exchange and thermolysis of several alkali metal titanate structure, Solid State Ionics 28–30 (1988) 1338–1343.
[27] A.R. Armstrong, G. Armstrong, J. Canales, P.G. Bruce, TiO_2-B nanowires, Angew. Chem. Int. Ed. 43 (2004) 2286–2288.
[28] H. Imai, Y. Takei, K. Shimizu, M. Matsuda, H. Hirashima, Direct preparation of anatase TiO_2 nanotubes in porous alumina membranes, J. Mater. Chem. 9 (1999) 2971–2972.
[29] Y.V. Kolen'ko, K.A. Kovnir, A.I. Gavrilov, A.V. Garshev, J. Frantti, O.I. Lebedev, B.R. Churagulov, G. Van Tendeloo, M. Yoshimura, Hydrothermal synthesis and characterization of nanorods of various titanates and titanium dioxide, J. Phys. Chem. B 110 (2006) 4030–4038.
[30] T. Ohsaka, F. Izumi, Y. Fujiki, Raman spectrum of anatase TiO_2, J. Raman Spectrosc. 7 (1978) 321–324.
[31] D. Bersani, P.P. Lottici, Phonon confinement effects in the Raman scattering by TiO_2 nanocrystals, Appl. Phys. Lett. 72 (1998) 73–75.
[32] D.V. Bavykin, B.A. Cressey, M.E. Light, F.C. Walsh, An aqueous, alkaline route to titanate nanotubes under atmospheric pressure conditions, Nanotechnology 19 (2008) 1–5.
[33] M. Kosmulski, The significance of the difference in the point of zero charge between rutile and anatase, Adv. Colloid Interface Sci. 99 (2002) 255–264.
[34] W.M. Wendl, G.H. Harry, Reflectance Spectroscopy, Interscience Publishers, John Wiley, New York/London/Sydney, 1996.
[35] B. Sun, A.V. Vorontsov, G. Smirniotis, Role of platinum deposited on TiO_2 in phenol photocatalytic oxidation, Langmuir 19 (2003) 3151–3156.
[36] A. Zachariah, K.V. Baiju, S. Shukla, K.S. Deepa, J. James, K.G.K. Warrier, Synergistic effect in photocatalysis as observed for mixed-phase nanocrystalline titania processed via sol–gel solvent mixing and calcinations, J. Phys. Chem. C 112 (2008) 11345–11356.
[37] J.G. Yu, H.G. Yu, B. Cheng, X.J. Zhao, Q.J. Zhang, Preparation and photocatalytic activity of mesoporous anatase TiO_2 nanofibers by a hydrothermal method, J. Photochem. Photobiol. A: Chem. 182 (2006) 121–127.
[38] L. Cao, A. Huang, F.J. Spiess, S.L. Suib, Gas-phase oxidation of 1-butene using nanoscale TiO_2 photocatalysts, J. Catal. 188 (1999) 48–57.
[39] A.V. Vorontsov, A.A. Altynnikov, E.N. Savinov, E.N. Kurkin, Correlation of TiO_2 photocatalytic activity and diffuse reflectance spectra, J. Photochem. Photobiol. A: Chem. 144 (2001) 193–196.
[40] Y.B. Mao, S.S. Wong, Size- and shape-dependent transformation of nanosized titanate into analogous anatase titania nanostructures, J. Am. Chem. Soc. 128 (2006) 8217–8226.
[41] S.R. Zheng, Z.Y. Xu, Y.D. Wang, Z.B. Wei, B.K. Wang, On the enhanced catalytic activity of TiO_2-supported layered compounds for Cr(VI) photo-reduction, J. Photochem. Photobiol. A: Chem. 137 (2000) 185–189.
[42] J.J. Testa, M.A. Grela, M.I. Litter, Experimental evidence in favor of an initial one-electron-transfer process in the heterogeneous photocatalytic reduction of chromium(VI) over TiO_2, Langmuir 17 (2001) 3515–3517.
[43] M. Gratzel (Ed.), Energy Resources through Photochemistry and Catalysis, Academic Press, New York, 1983.
[44] F. Jiang, Z. Zheng, Z.Y. Xu, S.R. Zheng, Z.B. Guo, L.Q. Chen, Aqueous Cr(VI) photoreduction catalyzed by TiO_2 and sulfated TiO_2, J. Hazard. Mater. B134 (2006) 94–103.
[45] S.R. Zheng, D.Q. Yin, W. Miao, G.K. Anderson, Cr(VI) photoreduction catalysed by ion-exchangeable layered compounds, J. Photochem. Photobiol. A: Chem. 117 (1998) 105–109.
[46] A. Kleinhammes, G.W. Wagner, H. Kulkarni, Y. Jia, Q. Zhang, L.C. Qin, Y. Wu, Decontamination of 2-chloroethyl ethylsulfide using titanate nanoscrolls, Chem. Phys. Lett. 411 (2005) 81–85.